Received: 15 December 2022 | Revised: 28 February 2023 | Accepted: 13 March 2023

DOI: 10.1002/elps.202200287

ELECTROPHORESIS

RESEARCH ARTICLE

Three-dimensional lab-on-a-foil device for dielectrophoretic separation of cancer cells

Mengren Wu[1] | **Yuan Gao**[1,2] | **Qiyue Luan**[3] | **Ian Papautsky**[3] | **Xiaolin Chen**[4] | **Jie Xu**[1]

[1]Department of Mechanical and Industrial Engineering, University of Illinois Chicago, Chicago, Illinois, USA

[2]Department of Mechanical Engineering, University of Memphis, Memphis, Tennessee, USA

[3]Department of Biomedical Engineering, University of Illinois Chicago, Chicago, Illinois, USA

[4]School of Engineering and Computer Science, Washington State University, Vancouver, Washington, USA

Correspondence
Jie Xu, Department of Mechanical and Industrial Engineering, University of Illinois at Chicago, Chicago, IL 60607, USA.
Email: jiexu@uic.edu

Color online: See article online to view Figures 1–5 in color.

Funding information
National Science Foundation, Grant/Award Numbers: 1917295, 1917299

Abstract

A simple, low-cost, three-dimensional (3D) lab-on-a-foil microfluidic device for dielectrophoretic separation of circulating tumor cells (CTCs) is designed and constructed. Disposable thin films are cut by xurography and microelectrode array are made with rapid inkjet printing. The multilayer device design allows the studying of spatial movements of CTCs and red blood cells (RBCs) under dielectrophoresis (DEP). A numerical simulation was performed to find the optimum driving frequency of RBCs and the crossover frequency for CTCs. At the optimum frequency, RBCs were lifted 120 μm in z-axis direction by DEP force, and CTCs were not affected due to negligible DEP force. By utilizing the displacement difference, the separation of CTCs (modeled with A549 lung carcinoma cells) from RBCs in z-axis direction was achieved. With the nonuniform electric field at optimized driving frequency, the RBCs were trapped in the cavities above the microchannel, whereas the A549 cells were separated with a high capture rate of 86.3% ± 0.2%. The device opens not only the possibility for 3D high-throughput cell separation but also for future developments in 3D cell manipulation through rapid and low-cost fabrication.

KEYWORDS
3D multilayer microfluidic device, CTCs separation, dielectrophoresis, lab-on-a-foil

1 | INTRODUCTION

Although the death rates from cancer declined by 27% from 1999 to 2019, cancer was still the second leading cause of death in the United States in 2019 [1, 2]. Metastasis is responsible for around 90% of cancer deaths [3]. In metastasis, cancer cells spread from the original (primary) tumor to another part of the body forming a new tumor in organs or tissues [4, 5]. The cells that break away and detach from the primary tumor, travel through vasculature or lymphatics, are called circulating tumor cells (CTCs) [6]. CTCs can serve as a biomarker for the diagnosis and potential therapy of cancers or tumors by providing real-time *in vitro* information [7]. Based on the number of CTCs in the peripheral blood of patients, cancer progression can be monitored by evaluating cancer prognosis and relapse [8]. In addition, the main treatment methods for cancer/tumor patients are gradually shifting from conventional standards to personalized techniques [9]. If CTCs

Abbreviations: CTCs, circulating tumor cells; RBCs, red blood cells; ROI, region of interest.

can be sorted from blood cells without biochemical labels, the clinical analysis of these cells can help with the development of personalized cancer treatment [5]. Therefore, there is a strong need for separating the CTCs from blood cells to diagnose and assess early-stage cancer. Although many macroscale isolation methods such as size-based filtration, density-based centrifugation, and immunocapture have been developed in recent years, these methods are limited by low capture rate and lack of automation [10]. For this purpose, the rapid microscale separation technology in miniaturized devices has attracted interest for CTCs isolation and downstream analysis of CTCs.

Indeed, recent development of miniaturization technologies has enabled microfluidic devices to offer a unique opportunity for manipulating cells at microscale due to their low volume requirement, high controllability, and biocompatibility. In addition, microfluidic devices can utilize external energy in cell manipulation, such as electric, acoustic, magnetic, and optic energies. In particular, the effectiveness of electric field is often amplified at the microscale, resulting in a wide range of applications for electrokinetics in manipulating cells [11–15]. Electrokinetics is the general term to describe the effect of electric field on the movement of fluids and particles suspended in fluids, including electrophoresis (EP), electroosmosis (EO), and dielectrophoresis (DEP). Different from linear EP and EO originating from Debye screening cloud of fixed counter ionic charge, DEP is a nonlinear electrokinetic phenomenon where the electric field acts on its own induced bipolar surface charge due to Maxwell–Wagner interfacial polarization. In the nonuniform electric field, DEP can produce effective dipole moment of cells by inducing charges at the membrane-electrolyte interface [2, 10, 16–19]. As the DEP force can rapidly control the movement of cells in a microscale flow depending on dielectric properties of cells relative to fluids, the cell viability and capture rate are much higher than the conventional methods. With these advantages, the dielectrophoretic microfluidic device provides great potential to separate CTCs from blood sample and monitor CTCs for early-stage cancer diagnosis [20, 21].

To fabricate microfluidics with electrodes, lift-off thin-film metal deposition is commonly used in microelectrode array fabrication on glass substrate, and PDMS replica techniques are used for constructing microfluidic channels. However, this process usually requires a cleanroom environment that is expensive and time-consuming. Moreover, the glasses are brittle, not self-sealing, and relatively expensive for disposable devices in biological and medical applications [22]. In addition, the PDMS replica techniques [23, 24] are difficult to construct multilayered microfluidic channels [25, 26] for developing three-dimensional (3D) channel network in applications, such as cell spatial movement in electric field, 3D cell manipulation, and high-throughput cells sorting. Hence, rapid and low-cost multilayer dielectrophoretic microfluidic device manufacturing method is highly sought-after. Recently, a novel concept has emerged in the microfluidics field by using of lab-on-a-foil [27]. Unlike PDMS-based microfluidic devices, a lab-on-a-foil system is constructed by thin and flexible films, which not only allow for constructing different structures in each layer and observing particles movements in 3D but also allow for integration with the rapid fabrication method for microelectrode array in microfluidic devices. Various fabrication methods for lab-on-a-foil devices have been studied, such as micro-thermoforming, hot roller embossing, dry resist technologies laser micromachining, and xurography [28]. Among these methods, xurography is a simple and versatile approach for fabricating microfluidic channels on thin-film materials using a digital plotter on each layer. To integrate the electrokinetics in a lab-on-a-foil microfluidic chip, a novel approach is applied to combine inkjet microelectrode array on thin-film system for rapid prototyping multilayer dielectrophoretic microfluidic devices.

Herein, we developed a dielectrophoretic multilayer lab-on-a-foil device to study the spatial DEP movement of red blood cells (RBCs) and CTCs (modeled with A549 lung carcinoma cells) and conducted the continuous separation of A549 cells from RBCs. Based on theoretical single-shell model and numerical simulation, the crossover frequency of A549 cells under an AC DEP was estimated. To validate the configuration of nonuniform electric field, the motility of RBCs and A549 cells were tested based on region of interest (ROI) grayscale intensity analysis. The z-axis movements of RBCs and A549 cells were evaluated at various driving voltages. Finally, by applying the crossover frequency of the AC signal with desired driving amplitude, the A549 cells were continuously separated from RBCs sample, and the capture rate was evaluated.

2 | MATERIAL AND METHODS

2.1 | Device design and working mechanism

In this work, we designed a multilayer lab-on-a-foil device to spatially control RBCs position along z-axis and separated out A549 cells based on DEP (Figure 1A). This microfluidic device consists of four layers of thin-film materials, including a substrate layer with inkjet microelectrode array, microchannel layer, cavity layer, and cover layer. The substrate layer includes four straight parallel microelectrodes to create AC DEP when the electric

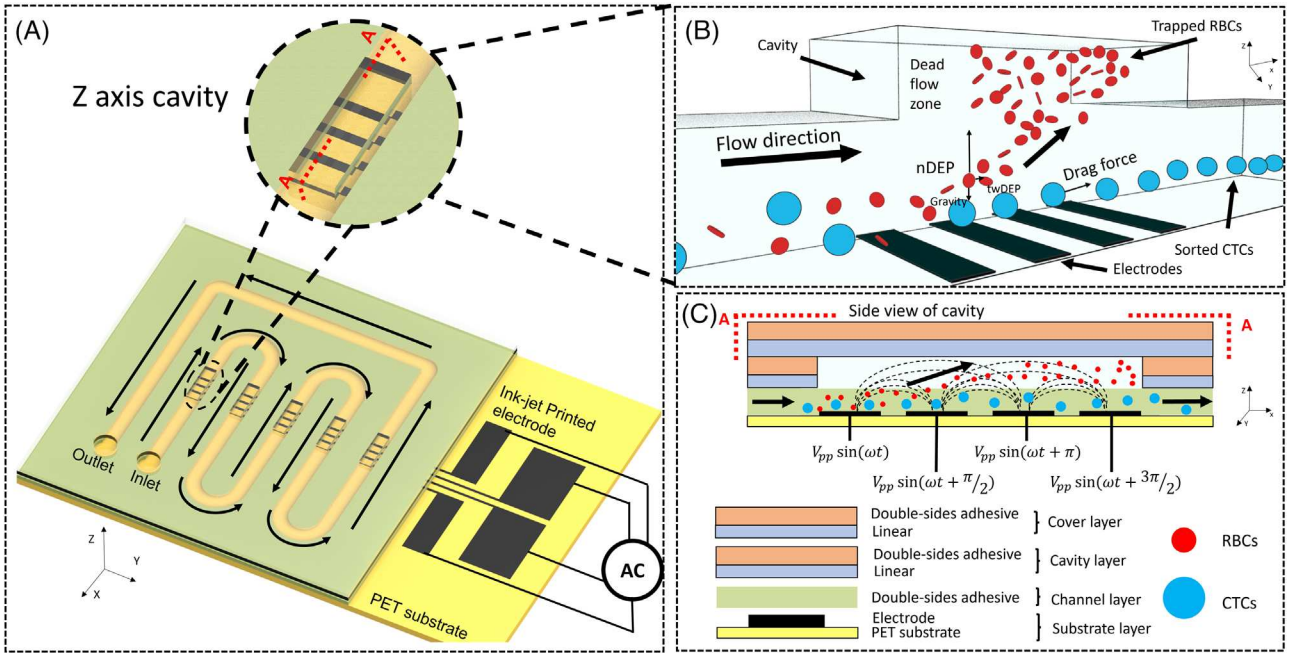

FIGURE 1 (A) Overview of the lab-on-a-foil multilayers microfluidic dielectrophoresis device for circulating tumor cells (CTCs) separation from red blood cells (RBCs). (B) Schematic illustration of separating process. (C) Cross-sectional illustration of multilayers device and separation process using nDEP.

signals with different phases are applied to the electrodes. In the microchannel layer, a serpentine-shape channel is designed for continuous large volume sample processing. Above the microfluidic layer, five rectangular cavities are designed the microchannel in the cavity layer to create dead flow zones that can trap and concentrate the RBCs cell inside the cavities. The cover layer is designed to enclose the microchannel, electrodes, and cavities with an inlet and an outlet, as shown in Figure 1A.

When the cell samples are injected from inlet with continuous flow, the AC driving signals are applied to this device and create a nonuniform field to induce DEP force on RBCs and A549 cells. By adjusting the applied frequency and phase on the electrodes, the DEP force on RBCs and A549 cells can be controlled based on their difference in the dielectric properties. The direction of nDEP force is positive along z–axis, and the gravity force is negative along z-axis, which is shown in Figure 1B. When electric signal is applied in the microchannel, both RBCs and A549 cells experience the DEP force along z-axis. In this device, at a specific range of frequencies, RBCs are lifted to the cavity in the microchannel as they experience strong DEP force, whereas the A549 cells are not lifted as the DEP force is negligible. When the RBCs are lifted to the cavity, they enter a dead flow zone and thus are trapped in the cavities. On the contrary, A549 cells will not be trapped and continue to flow to the outlet by the drag force. Therefore, the continuous separation of the A549 cells from the blood flow is realized in this device.

2.2 | Theory background

Based on the configuration of microelectrodes array, the DEP force F_{DEP} and twDEP force F_{twDEP} are induced on A549 cells and RBCs [16, 29–31]. The former force (F_{DEP}) causes the motion of the particles in the nonuniform electric field which is induced by interaction between the polarized particle and surrounding solution with spatial gradient of the electric field. The time-averaged DEP force can be defined as

$$F_{DEP} = 2\pi r^3 \varepsilon_m Re\left[f_{CM}(\omega)\right] \nabla \left|\vec{E}\right|^2 \quad (1)$$

where $\varepsilon_m$represents the permittivity of the medium, r is the radius of the particle, and $\nabla|\vec{E}|^2$ is the gradient of the squared magnitude of the electric field. The latter force F_{twDEP} acts to move the particle against or along the direction of the phase gradient, which can be calculated by

$$F_{twDEP} = 2\pi r^3 \varepsilon_m Im\left[f_{CM}(\omega)\right] \Sigma \left|\vec{E}\right|^2 \nabla\phi \quad (2)$$

and $\Sigma|\vec{E}|^2\nabla\phi$ is phase gradient factor. $Re[f_{CM}(\omega)]$ and $Im[f_{CM}(\omega)]$ are real and imaginary part of the Clausius–Mossotti (CM) factor (f_{CM}), respectively. Depending on whether $Re[f_{CM}(\omega)]$ is positive or negative, DEP force drives cells toward either strong field regions or weak field regions above the electrodes. Similarly, the twDEP force

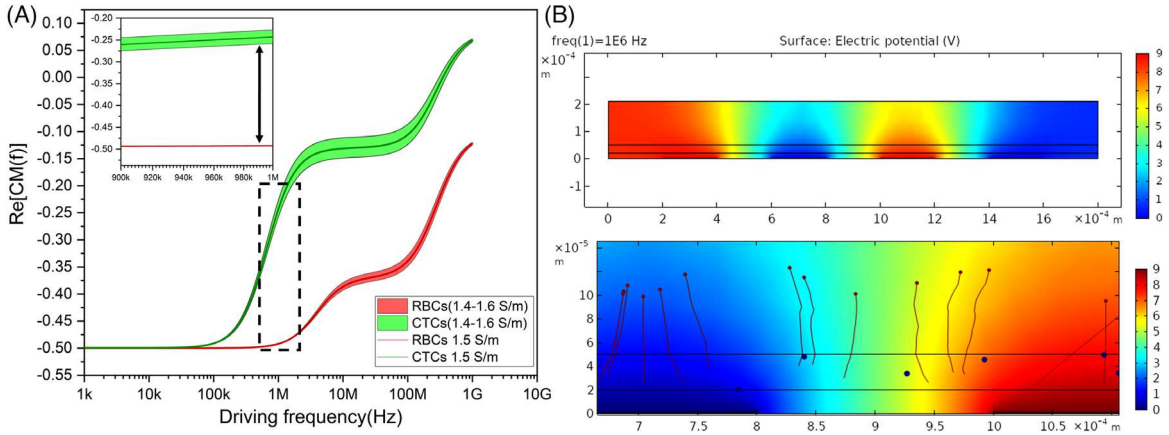

FIGURE 2 (A) Results of real part of Clausius–Mossotti (CM) factor calculation for carrier medium with 1.4–1.6 S/m. (B) The simulation results of electric field distribution and the trajectory of red blood cells (RBCs) (red) and A549 cells (blue). The trajectory results are a zoomed-in view of electric field distribution.

drives the particles along or against the direction of the phase gradient, depending on the sign of $Im[f_{CM}(\omega)]$ and the phase gradient factor $\Sigma E^2 \nabla\phi$ [16, 29, 30]. CM factor (f_{CM}) depends on the electrical properties (conductivity σ and permittivity ε) of the particle and its surrounding fluid, which can be calculated by

$$f_{CM} = \frac{\varepsilon_p^* - \varepsilon_m^*}{\varepsilon_p^* + 2\varepsilon_m^*} \tag{3}$$

where ε_p^* and ε_m^* indicate the complex permittivity of the particle and the surrounding medium, respectively. If the single-shell model is applied in calculating the complex permittivity of cell, the complex permittivity of particles ε_p^* is replaced by equivalent complex relative permittivity ε_{eq}^* based on the shell and interior properties of the cell:

$$\varepsilon_{eq}^* = \varepsilon_m^* \frac{\left(\frac{r_0}{r_i}\right)^3 + 2\left(\frac{\varepsilon_{cp}^* - \varepsilon_m^*}{\varepsilon_{cp}^* + 2\varepsilon_m^*}\right)}{\left(\frac{r_0}{r_i}\right)^3 - \left(\frac{\varepsilon_{cp}^* - \varepsilon_m^*}{\varepsilon_{cp}^* + \varepsilon_m^*}\right)} \tag{4}$$

where r_0 is the outer radius of cell, and r_i is the inner radius of cell (cytoplasm) ($r_i = r_0 - th_m$); th_m is the thickness of cell membrane; ε_{cp}^* and ε_m^* are complex permittivity of cytoplasm and cell membrane, respectively. The complex permittivity ε^* is dependent on electric frequency, relative permittivity, and conductivity, which can be defined $\varepsilon^* = \varepsilon - i(\sigma/\omega)$ [18, 32–34]. When CM factor is zero at the specific driving frequency, this frequency called crossover frequency and there is no DEP force applying on cells in suspending medium liquid. It also worth noting that when the levitation height of cells above electrodes is higher than the half of sum of electrodes width and spacing distance of two electrodes, the twDEP force is ignorable [16].

3 | RESULTS AND DISCUSSION

3.1 | Numerical simulation

The MyDEP [35], an open-source computational tool, was used for calculating the CM-factors of two different types of cells. The frequency-sweep-test and single-shell sphere model of cells were applied in calculation. The carrier medium properties were set based on the measurement results. As to two types of cells, the dielectric properties were referred to previous work [33, 36–38], including two types of properties based on classical and electrical model for describing cell membrane, and the detail can be found in Table S1. After sweep-test of CM factor, we numerically simulated the electric field and particles (RBCs and A549 cells) trajectory using COMSOL Multiphysics 5.4 to verify the principles of the device. In this process, the AC module and DEP in the particle tracing module were applied to a 2D geometry model that has the device dimension. The time-dependent calculator was used to calculate nonuniform electric field distribution and z-axis trajectory.

To find the crossover frequency for A549 cells and realize the optimal DEP performance on separating of A549 cells from RBCs, the CM-factors of two types of cells are calculated. The driving frequency ranges from 1 kHz to 1000 MHz, and a single-shell 2D sphere model was applied in medium with conductivity from 1.4 to 1.6 S/m with an increment of 0.1 S/m. We found that the frequency around 1×10^6 Hz is close to the crossover frequency of A549 cells and has the largest DEP force difference between two types of cells, allowing nDEP to lift RBCs and keep A549 cells at the bottom, which is shown in Figure 2A. Moreover, to validate the movement of cells under optimal frequency, the same parameters of cell and medium were used to in the simulation. Figure 2B shows the geometry dimension and

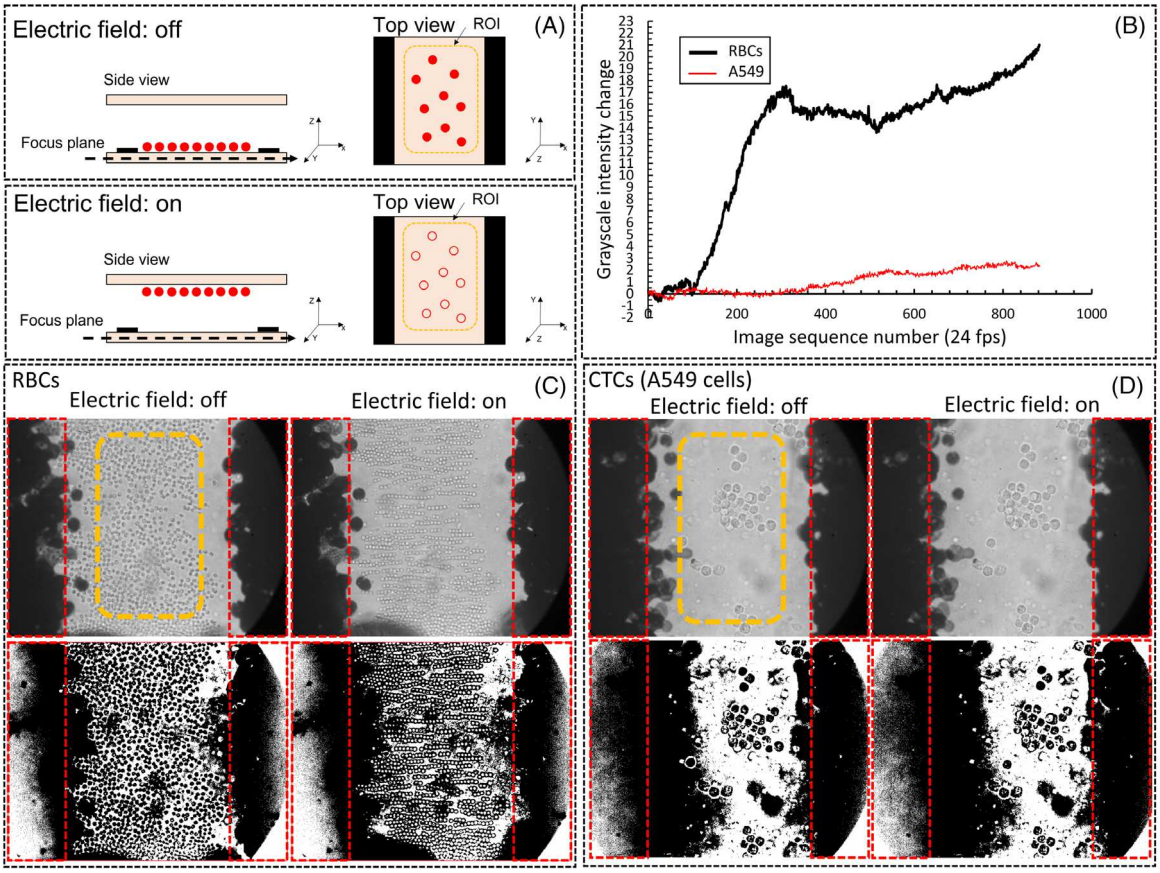

FIGURE 3 Process of evaluating *z*-axis direction movement (A) Illustration of intensity change in ROI with/without electric field when focus plane is fixed at the substrate of microchannel. (B) Results of intensity change of red blood cells (RBCs) and A549 cells. (C and D) Results of binary processing of RBCs and A549 cells.

electric field simulation results. After calculating the electric field, the single-shell model was used to describe A549 cells and RBCs. The initial position of cells was randomly distributed in the channel layer (black rectangular frame in simulation results), which is shown in Figure 2B. When the electric field is applied in this domain, the RBCs (red particles Figure 2B) start to move to the upper layer of the channel, whereas A549 cells maintain a lower position.

3.2 | Evaluation of *z*-axis movement based on grayscale microscope image sequence

To investigate and characterize the movement and displacement of cells along *z*-axis, we separately infused the RBCs and A549 cells sample into the microfluidic device and sedimented cells to microchannel substrate without flow. Meanwhile, the focus plane was set on microchannel substrate to capture *z*-axis displacement of cells under DEP force. Once the cells start moving along the *z*-axis to the top of channel, the grayscale intensity of each cell changed because the position of the cells is different from the focal plane, which is shown in Figure 3A. In this process, the original image of the cells is converted to binary grayscale. To quantify the change of grayscale intensity during the cell movement, an ROI was defined between two electrodes (dot line rectangular in Figure 3C,D). When cells move away from the bottom electrodes and focal plane, the cell membrane becomes darker than cytoplasm and cytoplasm turns to white. At this moment, grayscale intensity of ROI increases depending on distance between cells and the focal plane. Therefore, the variation in the grayscale intensity of ROI was suggested to quantitatively analyze the cell position.

For the purpose of evaluation of *z*-axis moving, the locations of cells were captured by a high-speed camera and converted to an image sequence. After that, the ROI with the same area was defined for each image, and all sets of images were converted to 8-bit grayscale using open-source software ImageJ/Fiji (NIH, USA). Figure 3C,D shows the original images and processed images of RBCs and A549 cells between two electrodes with and without an electric field. By quantitatively analyzing the average intensity in the ROI, we compared the average intensity change (I_{ROI}) for RBCs and A549 cells at 1 MHz, which is close to

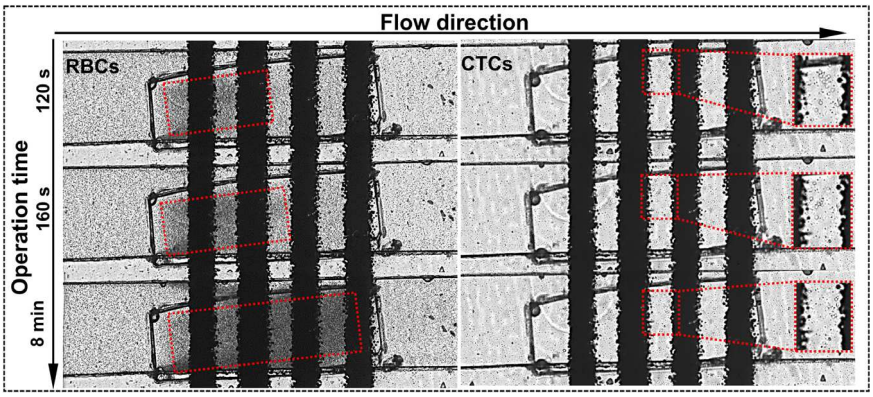

FIGURE 4 Trapping performance for red blood cells (RBCs) and A549 cells at 120 s, 160 s, and 8 min.

the theoretical crossover frequency. Figure 3B shows that under the DEP electric field, I_{ROI} of blood cells increased to maximum value ($\Delta I_{ROI} \approx 18$ *in grascale intensity*), whereas I_{ROI} of CTCs kept constant (~2) within 320 frames (~13 s in 24 frames per second recording).

3.3 | Evaluation of trapping and separation performance

To validate the spatial transport of cells in a continuous flow, the samples of RBCs and A549 cells were separately injected in this device with the same flow rate. Based on the previous results, the AC electric field was conducted with the driving signal of 900 mVpp and 1 MHz. To ensure consistency in the experimental conditions, the observation window was set on the same cavity and electrode array. By applying a frequency of 1 MHz, the image sequence of the cavity was captured after turning the electric field at 120 s, 160 s, and 8 min. The results indicate that RBCs were trapped in the cavity and the number of trapped RBCs increased with time as the cells were moving to the dead zone of flow by DEP force (Figure 4). Moreover, the different grayscale intensities in the microcavity were observed before and after applying electric field due to concentration change of RBCs. On the contrary, the A549 cells were not trapped in the cavities, and intensity of cavities was not changed. This result is consistent with the results of the z-axis moving test. At the crossover frequency (1 MHz), the DEP force on A549 cells is too weak to make A549 cells move along z-axis, whereas RBCs experienced strong DEP force, and thus, they were lifted by DEP force. With the external fluid field, A549 cells experienced drag force and flowed with bottom streaming to outlet, whereas RBCs lifted to the cavities and trapped in the cavities where they will not be influenced by the fluid flow. It is worth noting that cells in the one single cavity, some RBCs went out of cavities after 8 min due to the capacity of trapping blood. The capacity of entire device can be enhanced by adding more cavity unit along with the micro channel.

After separately testing on the trapping performance for two types of cells, the mixture of two types of cells sample was applied in the device to demonstrate and evaluate the separation efficiency of A549 cells. The sample was first counted in hemocytometer and then was injected in the microchannels through a syringe pump at flow rate 1 μL/min. When the flow of sample is stable, the 1 MHz with 900 mVpp driving single was applied on five electrode arrays. After passing all five cavities with DEP area and moving to the outlet, the separated sample was pipetted out and transferred to the hemocytometer to count cell numbers. The cell distribution in channel before/after applying the DEP field can be found in Figure S5. The capture rate of A549 cells was then evaluated by cell counting process. The results in Figure 5C show that the A549 cells percentage in sample with/without being processed in the device. The A549 cells percentage is enhanced from 2.0% ± 0.6% to 86.3% ± 0.2%. As shown in Figure 5D, the A549 cells capture rates were evaluated, and the results show 80.0% ± 10.0%, 82.7% ± 1.3%, and 86.3% ± 0.2% with a total cell number of 10, 100, and 1000, respectively.

4 | CONCLUDING REMARKS

In summary, a novel low-cost dielectrophoretic microfluidic device was developed for separating CTCs (A549 cells) from RBCs. The device was made of off-the-shelf PET films and medicalgrade double-sided tapes with xurography technique, and the microelectrode array was made by inkjet technique using nanoparticle conductive ink. Compared with regular lift-off and mode replica techniques, our fabrication method for electrophoretic device provides a rapid, low-cost way for prototyping microfluidic devices without cleanroom requirement. The device allowed for different designs of microchannel along z-axis to observe spatial movements of cells.

The optimal operating frequency of the device was determined to be 1 MHz through a numerical simulation involving a frequency-sweep-test. At this frequency,

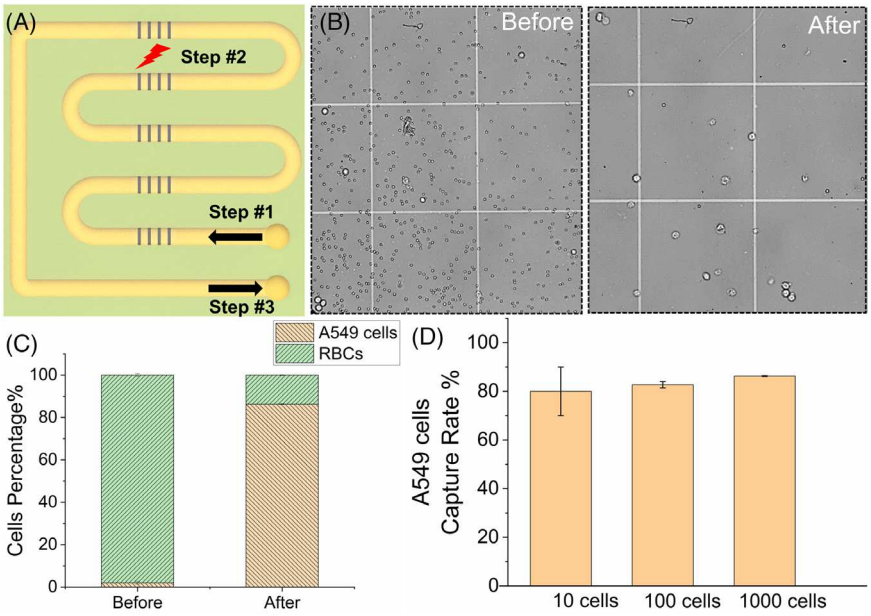

FIGURE 5 (A) IIllustration of separation procedure including three steps: (1) infuse mixture samples, (2) apply electric field, and (3) collect separated samples. (B) Image of sample before and after separation. (C) Cell percentage of sample before and after separation process. (D) A549 cells capture rate in 10, 100, and 1000 cells.

the A549 cells remained at the bottom of the microchannel, whereas the RBCs entered the cavities above the channel. The experimental investigation of the *z*-axis displacement of A549 cells and RBCs was conducted based on the grayscale intensity test in the ROI. The study found that the intensity of the ROI changes with the movement of cells when the focal plane is fixed, which makes it possible to examine the movement of cells along the *z*-axis. Additionally, the intensity of the ROI was used to measure cell displacement through adjusting focal plane. The results show that under conditions of 1 MHz and 900 mVpp, RBCs were lifted 120 μm by nDEP force, whereas A549 cells did not show significant displacement. These findings were consistent with the numerical simulation results, indicating that the inkjet-based lab-on-a-foil microfluidic device is effective in separating different types of cells. Based on these findings, we optimized the device to separately investigate the trapping performance for A549 cells and RBCs in a continuous flow at 1 μL/min. The results show that RBCs are trapped in cavities, and the maximum capability is achieved when operating time is 8 min, whereas no A549 cells are trapped in the same conditions. Finally, the mixture of A549 cells and RBCs was infused in the device to demonstrate A549 cell separation, and the capture rate achieves 86.37% ± 0.2%.

To the best of our knowledge, this is the first demonstration of spatially separating A549 cells along depth direction of a microfluidic channel in a multilayer microfluidic device. This work not only provides a promising lab-on-a-foil microfluidic platform for studying spatial movement of cells in DEP through a rapid and low-cost fabrication method but also for future development of cell and particle separation in multilayer dielectrophoretic microfluidic devices. Additionally, the multilayer device used in this study offers versatility in design, allowing for different layers to be utilized, which offers a method to 3D manipulate cells with DEP. The selective control of cell movement in *z*-axis has great potential for various biomedical applications such as cell separation, 3D cell patterning for cancer diagnosis, and screening.

ACKNOWLEDGMENTS

This work is supported by the National Science Foundation under Grant No. 1917295 and No. 1917299. Mengren Wu thanks the support from the Graduate Research/Deiss Award in Biomedical Graduate Research.

CONFLICT OF INTEREST STATEMENT

The authors have declared no conflict of interest.

DATA AVAILABILITY STATEMENT

The data that support the findings of this study are available in the Supporting Information of this article.

ORCID

Mengren Wu https://orcid.org/0000-0002-7059-4305
Yuan Gao https://orcid.org/0000-0002-5464-1626
Qiyue Luan https://orcid.org/0000-0003-4047-9856
Ian Papautsky https://orcid.org/0000-0002-1396-9625
Xiaolin Chen https://orcid.org/0000-0002-8760-6480
Jie Xu https://orcid.org/0000-0001-5765-7431

REFERENCES

1. An Update on Cancer Deaths in the United States. Centers for disease control and prevention. 2021. https://www.cdc.gov/cancer/dcpc/research/update-on-cancer-deaths/index.htm
2. Gascoyne PR, Vykoukal J. Particle separation by dielectrophoresis. Electrophoresis. 2002;23(13):1973–83.

3. Seyfried TN, Huysentruyt LC. On the origin of cancer metastasis. Crit Rev Oncog. 2013;18(1–2):43–73.
4. Gupta GP, Massagué J. Cancer metastasis: building a framework. Cell. 2006;127(4):679–95.
5. Toss A, Mu Z, Fernandez S, Cristofanilli M. CTC enumeration and characterization: moving toward personalized medicine. Ann Transl Med. 2014;2(11):108.
6. Riquet M, Rivera C, Gibault L, Pricopi C, Mordant P, Badia A, et al. Lymphatic spread of lung cancer: anatomical lymph node chains unchained in zones. Rev Pneumol Clin. 2014;70(1–2):16–25.
7. Yu L, Ng SR, Xu Y, Dong H, Wang YJ, Li CM. Advances of lab-on-a-chip in isolation, detection and post-processing of circulating tumour cells. Lab Chip. 2013;13(16):3163–82.
8. Mocellin S, Hoon D, Ambrosi A, Nitti D, Rossi CR. The prognostic value of circulating tumor cells in patients with melanoma: a systematic review and meta-analysis. Clin Cancer Res. 2006;12(15):4605–13.
9. Krebs MG, Hou J-M, Ward TH, Blackhall FH, Dive C. Circulating tumour cells: their utility in cancer management and predicting outcomes. Ther Adv Med Oncol. 2010;2(6):351–65.
10. Li P, Stratton ZS, Dao M, Ritz J, Huang TJ. Probing circulating tumor cells in microfluidics. Lab Chip. 2013;13(4):602–9.
11. Xuan X. Recent advances in direct current electrokinetic manipulation of particles for microfluidic applications. Electrophoresis. 2019;40(18–19):2484–513.
12. Xuan X. Review of nonlinear electrokinetic flows in insulator-based dielectrophoresis: from induced charge to Joule heating effects. Electrophoresis. 2022;43(1–2):167–89.
13. Song M, Lin X, Peng Z, Zhang M, Wu J. Enhancing affinity-based electroanalytical biosensors by integrated AC electrokinetic enrichment—a mini review. Electrophoresis. 2022;43(1–2):201–11.
14. Yao J, Zhu G, Zhao T, Takei M. Microfluidic device embedding electrodes for dielectrophoretic manipulation of cells—a review. Electrophoresis. 2019;40(8):1166–77.
15. Perez-Gonzalez VH. Particle trapping in electrically driven insulator-based microfluidics: dielectrophoresis and induced-charge electrokinetics. Electrophoresis. 2021;42(23):2445–64.
16. Pethig RR. Dielectrophoresis: theory, methodology and biological applications. Hoboken, NJ: John Wiley and Sons; 2017.
17. Lewpiriyawong N, Yang C. AC-dielectrophoretic characterization and separation of submicron and micron particles using sidewall AgPDMS electrodes. Biomicrofluidics. 2012;6(1):012807.
18. Jones TB. Electromechanics of particles. Cambridge: Cambridge University Press; 1995.
19. Pohl HA, Crane JS. Dielectrophoresis of cells. Biophys J. 1971;11(9):711–27.
20. Chan JY, Ahmad Kayani AB, Md Ali MA, Kok CK, Majlis BY, Hoe SLL, et al. Dielectrophoresis-based microfluidic platforms for cancer diagnostics. Biomicrofluidics. 2018;12(1):011503.
21. Ramirez-Murillo CJ, de los Santos-Ramirez JM, Perez-Gonzalez VH. Toward low-voltage dielectrophoresis-based microfluidic systems: a review. Electrophoresis. 2021;42(5):565–87.
22. Fallahi H, Zhang J, Phan HP, Nguyen NT. Flexible microfluidics: fundamentals, recent developments, and applications. Micromachines. 2019;10(12):830.
23. Rogers JA, Nuzzo RG. Recent progress in soft lithography. Mater Today. 2005;8(2):50–6.
24. Kim P, Kwon KW, Park MC, Lee SH, Kim SM, Suh KY. Soft lithography for microfluidics: a review. Biochip J. 2008;2:1–11.
25. Glick CC, Srimongkol MT, Schwartz AJ, Zhuang WS, Lin JC, Warren RH, et al. Rapid assembly of multilayer microfluidic structures via 3D-printed transfer molding and bonding. Microsyst Nanoeng. 2016;2(1): 16063.
26. Zhang M, Wu J, Wang L, Xiao K, Wen W. A simple method for fabricating multi-layer PDMS structures for 3D microfluidic chips. Lab Chip. 2010;10(9):1199–203.
27. Focke M, Kosse D, Müller C, Reinecke H, Zengerle R, von Stetten F. Lab-on-a-foil: microfluidics on thin and flexible films. Lab Chip. 2010;10(11):1365–86.
28. Bartholomeusz DA, Boutté RW, Andrade JD. Xurography: rapid prototyping of microstructures using a cutting plotter. J Microelectromech Syst. 2005;14(6):1364–74.
29. Wang X-B, Huang Y, Becker F, Gascoyne P. A unified theory of dielectrophoresis and travelling wave dielectrophoresis. J Phys D: Appl Phys. 1994;27(7):1571.
30. Pethig R, Talary MS, Lee RS. Enhancing traveling-wave dielectrophoresis with signal superposition. IEEE Eng Med Biol Mag. 2003;22(6):43–50.
31. Peng Y, Li D, Yang X, Ma Z, Mao Z. A review on electrohydrodynamic (EHD) pump. Micromachines. 2023;14(2):321.
32. Cheng I-F, Huang W-L, Chen T-Y, Liu C-W, Lin Y-D, Su W-C. Antibody-free isolation of rare cancer cells from blood based on 3D lateral dielectrophoresis. Lab Chip. 2015;15(14):2950–9.
33. Turcan I, Olariu MA. Dielectrophoretic manipulation of cancer cells and their electrical characterization. ACS Comb Sci. 2020;22(11):554–78.
34. Liu W, Ren Y, Tao Y, Zhou Z, Wu Q, Xue R, et al. Multiple frequency electrothermal induced flow: theory and microfluidic applications. J Phys D: Appl Phys. 2020;53(17):175304.
35. Cottet J, Fabregue O, Berger C, Buret F, Renaud P, Frénéa-Robin M. MyDEP: a new computational tool for dielectric modeling of particles and cells. Biophys J. 2019;116(1):12–8.
36. Zhang Y, Chen X. Dielectrophoretic microfluidic device for separation of red blood cells and platelets: a model-based study. J Braz Soc Mech Sci Eng. 2020;42(2):1–11.
37. Wang K, Zhao Y, Chen D, Fan B, Lu Y, Chen L, et al. Specific membrane capacitance, cytoplasm conductivity and instantaneous Young's modulus of single tumour cells. Sci Data. 2017;4(1):170015.
38. Sudsiri CJ, Ritchie RJ. Energy absorption of human red blood cells and conductivity of the cytoplasm influenced by temperature. Biophys Chem. 2021;273:106578.

SUPPORTING INFORMATION

Additional supporting information can be found online in the Supporting Information section at the end of this article.

How to cite this article: Wu M, Gao Y, Luan Q, Papautsky I, Chen X, Xu J. Three-dimensional lab-on-a-foil device for dielectrophoretic separation of cancer cells. Electrophoresis. 2023;1–9. https://doi.org/10.1002/elps.202200287